Fusion Engineering and Design 230 (2026) 115909

Contents lists available at ScienceDirect

Fusion Engineering and Design

journal homepage: www.elsevier.com/locate/fusengdes

Neutronic and thermo-mechanical analysis in support of the design of the water-cooled lead ceramic breeder breeding blanket concept for the EU DEMO

G. Bongiovì [a,*], P. Chiovaro [a], I. Catanzaro [a], S. Maggio [a], F.A. Hernandez [b,c], S. D'Amico [b,c], E. Vallone [a], P.A. Di Maio [a]

[a] Department of Engineering, University of Palermo, Viale delle Scienze Ed. 6, Palermo, 90128, Italy
[b] Institut für Neutronenphysik und Reaktortechnik (INR), Karlsruher Institut für Technologie (KIT), Eggenstein-Leopoldshafen, 76344, Germany
[c] Fusion Technology Department - Programme Management Unit, EUROfusion Consortium, Boltzmannstraße 2, Garching, 85748, Germany

ARTICLE INFO

Keywords:
DEMO
WLCB
Breeding blanket
Neutronics
Thermomechanics

ABSTRACT

The Water-cooled Lead Ceramic Breeder (WLCB) Breeding Blanket (BB) concept is conceived in order to merge the Helium-Cooled Pebble Bed (HCPB) and the Water-Cooled Lithium Lead (WCLL) BB concepts, studied for a long time within the EUROfusion consortium, taking the best from each of them. The WLCB BB is characterised by the adoption of a solid breeder, molten lead as neutron multiplier and water at PWR conditions as coolant. Its design relies on the presence of actively cooled first wall and vertical stiffeners. Cassettes to clad functional materials are adopted as well. The ultimate scope is to develop a BB concept capable of fulfilling the high-level DEMO requirements with proven technology and acceptable risk level, overcoming the critical aspects characterising the WCLL and HCPB BB development. In this context, the University of Palermo is involved in the WLCB BB design in close cooperation with EUROfusion. Several architectures have been investigating over the years, to find the best in terms of heat removal, tritium breeding, shielding, structural integrity and manufacturing. In this paper, neutronic and thermo-mechanical analysis to sustain the WLCB BB design based on the baseline architecture are presented. From the nuclear standpoint, analysis to calculate the deposited heat power has been performed, considering either Eurofer or SiC as cassettes structural material. Afterwards, thermo-mechanical analysis of the Central Outboard Blanket segment Top Cap (TC) region has been performed, to obtain a robust layout of such a critical region under steady-state nominal conditions. To this scope, the impact of the non-ideal contact between cassettes and structural components on the segment thermo-mechanical performances has been assessed in detail. The obtained outcomes allowed highlighting the potential benefits of adopting SiC instead of Eurofer for the cassette and suggesting design improvements to increase the WLCB BB neutronic and thermo-mechanical performances.

1. Introduction

In order to design a Breeding Blanket (BB) system for the EU DEMO reactor capable of bridging the technology gap between ITER and the commercial fusion power plants, the EUROfusion consortium started the design of a "driver" BB system aimed at achieving high-level stakeholder requirements of tritium self-sufficiency and power extraction for net electricity production with proven technology and/or operational parameter [1]. To this purpose, two BB concepts have been chosen as candidate for DEMO driver BB: the Helium-Cooled Pebble Bed (HCPB) and the Water-Cooled Lithium lead (WCLL). They were down-selected at the end of the DEMO Pre-Conceptual Design phase, concluded in 2020 [2]. Although the intense research activities deployed to attain robust design of both HCPB and WCLL BB concepts in view of the DEMO requirements and despite the progress in design and performances, critical issues persist. Therefore, alternative BB concepts have been emerging over the last years, try combining the HCPB and WCLL features to develop a BB concept capable of mitigating risks and overcoming potential showstoppers. Among these alternatives, the most promising is the Water-cooled Lead Ceramic Breeder (WLCB) BB concept. It

* Corresponding author.
E-mail address: gaetano.bongiovi@unipa.it (G. Bongiovì).

https://doi.org/10.1016/j.fusengdes.2026.115909
Received 4 February 2026; Received in revised form 29 April 2026; Accepted 22 June 2026
Available online 27 June 2026

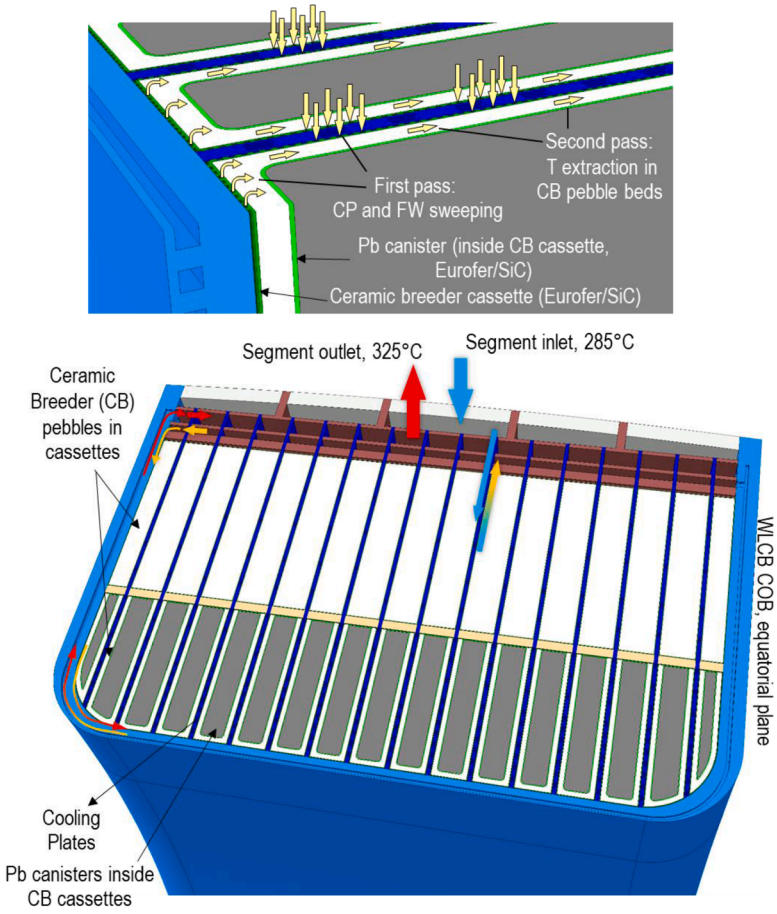

Fig. 1. View of the WLCB BB elementary unit of the COB segment.

represents the best compromise between HCPB and WCLL to mitigate and/or solve almost all the critical issues affecting the DEMO BB design so far.

The present paper finds its place in the design activities promoted by the EUROfusion consortium and devoted to design the WLCB BB for DEMO. In particular, the paper deals with neutronic and thermo-mechanical analysis performed at the University of Palermo, in close collaboration with the DEMO Central Team of EUROfusion, in support of the design of the WCLB BB Central Outboard Blanket (COB) segment, conceived according to the newest baseline architecture. In Section 2, a brief overview of the WLCB BB concept baseline architecture is given, whereas in Section 3 the campaign of neutronic analysis dedicated to evaluate the heat power and its volumetric density deposited by neutrons and gammas within the structural and functional materials is described, assuming two different options (Eurofer and SiC) for the cassette structural material. Then, in Section 4 and 5, the thermal and thermo-mechanical analysis of the Top Cap region of the WCLB BB COB segment is presented, describing the thermal and structural performances of the considered layout and assessing in detail the impact of the contact between cassette and structural components on the overall thermo-mechanical performances, highlighting the effect of the structural material considered for the cassettes. Finally, in Section 6, the conclusion is given.

2. The WLCB BB concept

The WLCB BB concept has been conceived in EUROfusion as a hybrid design, putting together the best characteristics of the HCPB and WCLL BB concepts to attain a robust BB system for the EU DEMO. Several WLCB BB architectures have been assessing in the last years [3–7] up to that addressed in this paper,which represent the current baseline, after multiple design steps.

The WLCB BB foresees water cooling at PWR conditions (285–325 °C @15.5 MPa), with the Breeding Zone (BZ) and the Segment Box (SB) being cooled in series. The Advanced Ceramic Breeder (ACB), consisting in a mixture of Li_4SiO_4 + 35% mol. Li_2TiO_3, 64% vol. fraction, enriched at 90% in ^6Li and produced with the KALOS process, in form of pebble bed is used as breeder whereas molten lead is adopted as neutron multiplier. A mixture of He and H_2/H_2O @0.2 MPa is used as purge gas to remove T from the BZ. It flows throughout the pebble beds making a double pass throughout the BZ. The WLCB BB geometric layout relies on the Single Module System architecture, to efficiently withstand electromagnetic loads and optimize neutronic performances and maintenance. The segment design is based on a multilayer First Wall (FW) composed of a tungsten plasma-facing armour (0.5 mm thick [8]) and a 25 mm wall with embedded cooling channels (square channels with a side of 7 mm). The FW is joined to 50 mm thick Sidewalls (SWs) through the bend regions, whose thickness vary along the curvature. Within each segment, a manifold system integrated in the BB structure within its Back Supporting Structure (BSS) is aimed at optimizing the space allocation and maximize shielding performances. FW, SWs, BSS and the Top and Bottom Caps form the SB. Moreover, vertical Cooling Stiffeners (CSs) 8 mm-thick are adopted to extract the thermal power from the BZ (through rectangular cooling channels of 5 × 10 mm section), contributing to ensure the blanket integrity. Vertical cassettes (2 mm-thick) that alternate ACB and molten Pb (separated by canisters 1.5 mm-thick) are located within the BZ, acting as cladding to house functional materials. Cassettes installation allow obtaining the purge gas channels, having a 1 × 2 mm rectangular section. Eurofer is presently assumed as cassettes and canisters structural material, considering the SiC as potential

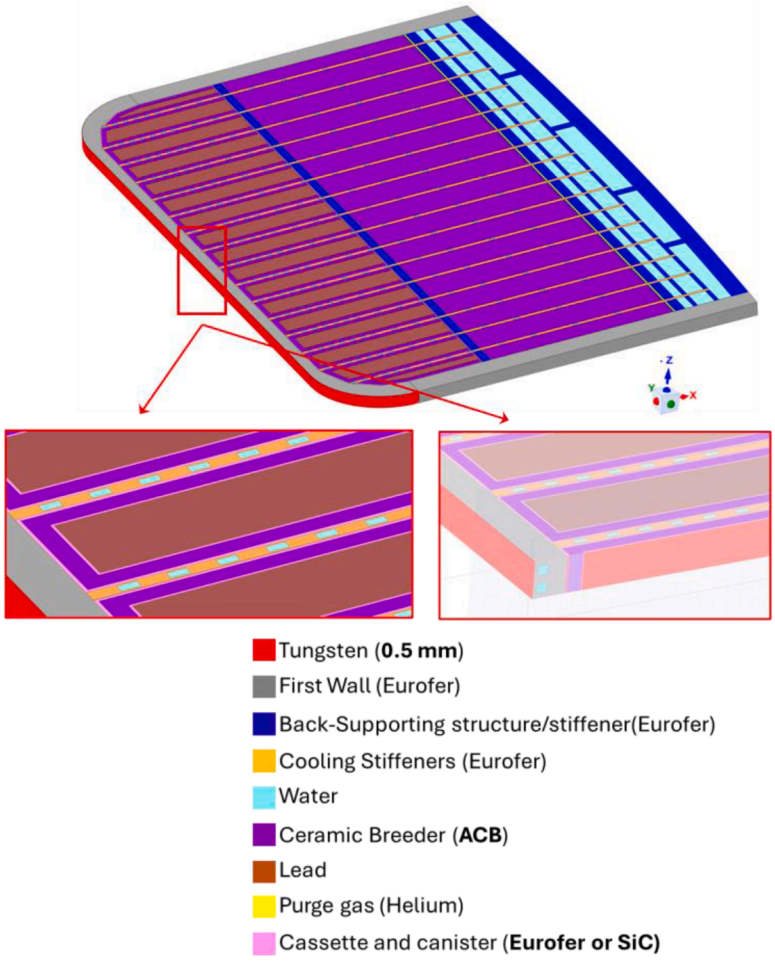

Fig. 2. WLCB BB COB segment equatorial slice simplified for nuclear analysis.

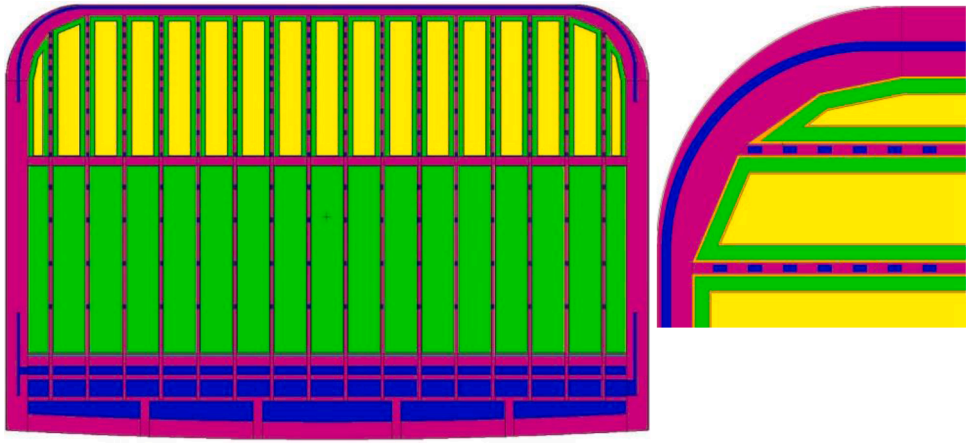

Fig. 3. MCNP model toroidal – radial section of the WLCB BB equatorial outboard slice.

alternative. As an example, a view of the WLCB BB elementary unit of the COB segment is provided in Fig. 1. It can be observed that the BZ is divided in two radial regions: the front one, from the FW to the poloidal-toroidal back plate (20 mm-thick) containing the molten Pb and breeder, extends for 325 mm whereas the second one, from the poloidal-toroidal back plate to the manifolds, extends for 432 mm and houses only breeder. Globally, the radial thickness of the outboard blanket in the reactor mid plane is 1000 mm, as per DEMO 2017–18 baselines.

3. Neutronic analysis

An intense campaign of neutronic analysis has been performed in order to characterise the nuclear behaviour of the WLCB BB, paying particular attention to the nuclear heating to be provided as input to the thermal analysis. To this end, nuclear calculations have been carried out using a computational approach based on the Monte Carlo method, by means of the Monte Carlo N-Particle (MCNP5.1.6) code [9] and the JEFF-3.3 libraries [10] for the transport cross-section.

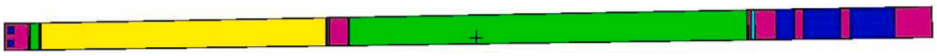

Fig. 4. MCNP model poloidal – radial section of the WLCB BB equatorial outboard slice.

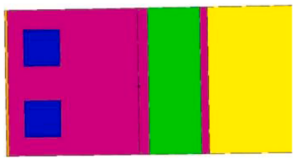

Fig. 5. Particular of the MCNP model poloidal – radial view of the WLCB BB equatorial outboard slice.

3.1. The geometric model

In order to develop an MCNP model of an equatorial section of the COB segment of the WLCB BB concept, based on the current baseline architecture, a proper geometric model has been considered. In particular, the assumed geometric layout represents a toroidal-radial slice of the equatorial region of the WLCB BB COB segment. It has been set-up with the necessary geometrical simplifications to strike a balance between the accuracy of the setup and the computational burden, bearing in mind the numerous analyses required for the complete nuclear characterisation of the WLCB BB. Specifically, the most significant geometric simplifications involve squaring of some rounded shapes and replacing the lead plasma front cassettes with cells made of a homogeneous material, so to remove the purge gas channels (shown in Fig. 1). Two different variants have been assessed, namely that foreseeing Eurofer cassettes and canisters (which is the baseline configuration) and the variant with these components made of SiC. In the model, a 0.5 mm thick tungsten layer has been assumed, with Eurofer as structural material, ACB for tritium production and molten Pb as neutron multiplier, spatially distributed as shown in Fig. 2.

3.2. The MCNP model

The WLCB BB nuclear behaviour has been assessed focussing on

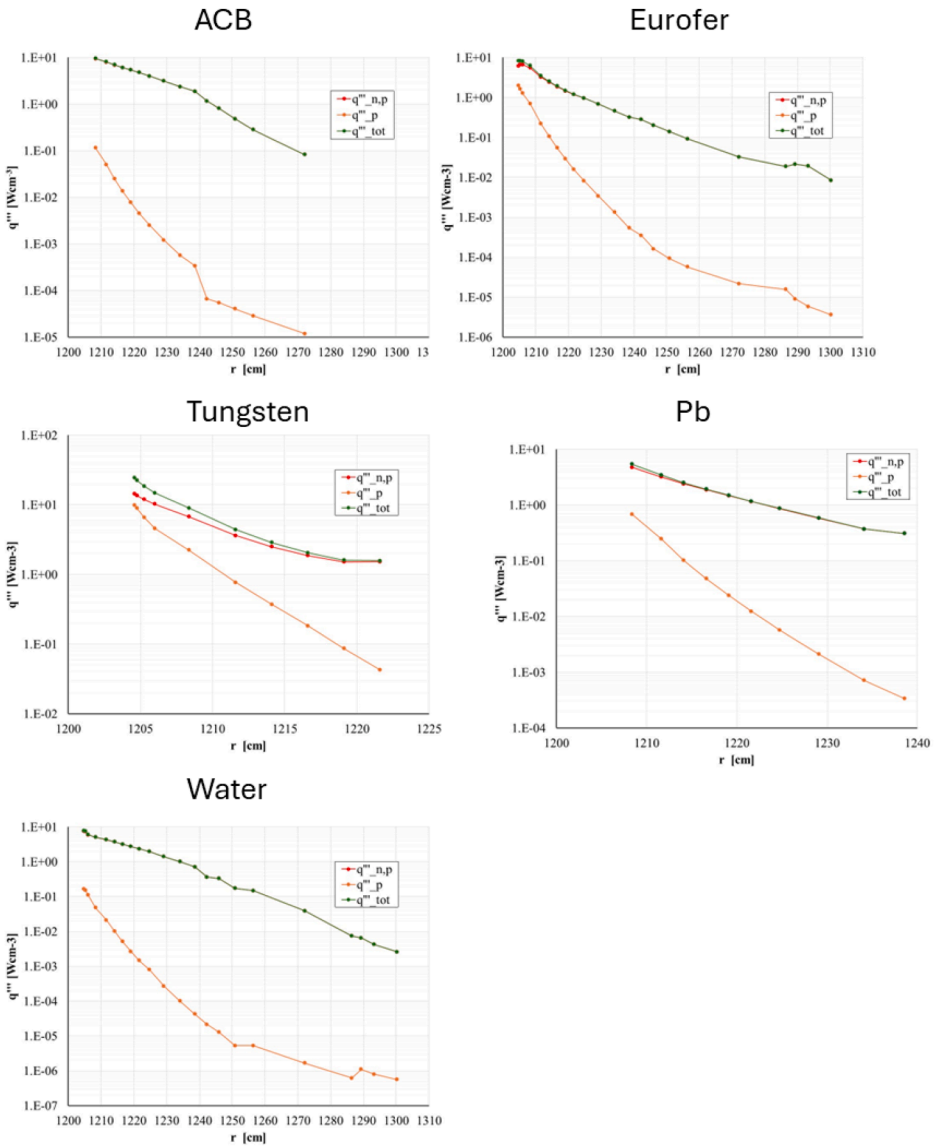

Fig. 6. Eurofer cassette option – volumetric heat power density along radial coordinate.

Table 1
Eurofer cassette option – total deposited power.

Material	Power [W]
ACB	2.10E+04
Eurofer	1.22E+04
Tungsten	4.56E+02
Lead	9.73E+03
Water	1.77E+03
Total Slice	**4.38E+04**
Total Slice – SiC cassette option	**4.53E+04**

nuclear heating that is the neutronic and photonic released power along with the spatial distribution of its volumetric density. Regarding the nuclear heating, the results are normalised to the yield of neutrons and photons related to DEMO fusion power (1.998 GW, as per DEMO 2017 baseline). The simplified geometry has been converted in the constructive solid geometry representation adopted by MCNP by means of SuperMC code [11] (Figs. 3, Figs. 4 and 5).

As far as boundary conditions are concerned, reflecting surfaces have been used in the poloidal and toroidal direction, respectively to consider the geometrical continuity in those directions [12–14]. Regarding the considered materials, EUROfusion guidelines and handbook [15] have been adopted. The DEMO irradiation conditions have been simulated defining a plasma-facing surface source for the slice model. A proper bias in cosines and energies has been set-up, adopting the same procedure reported in [12,13] that allows assessing the probability distribution of cosine and energy of the neutron and photon sources on the basis of a dedicated nuclear analysis, performed assuming the overall MCNP model of the DEMO machine endowed with the WLCB blanket. The obtained neutronic results are affected by a statistical error much

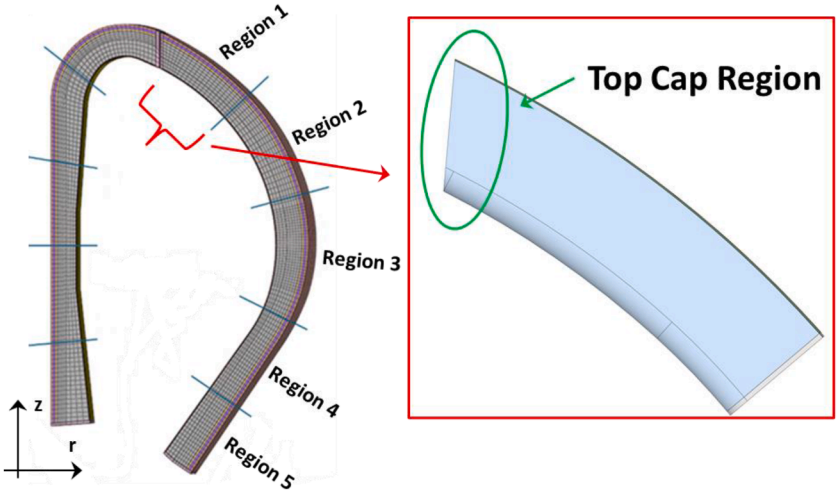

Fig. 7. WLCB COB and Top Cap Region.

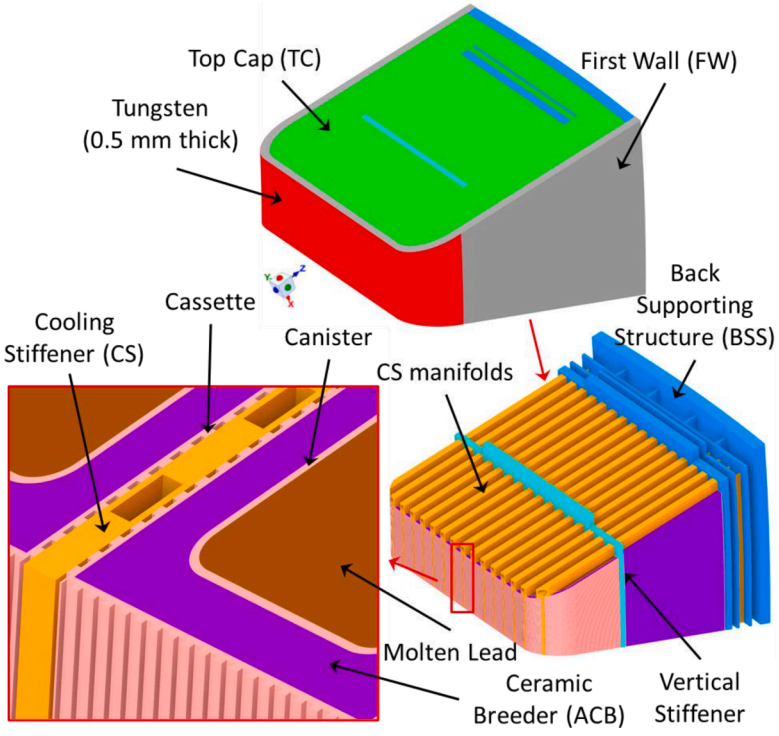

Fig. 8. The WLCB Top Cap region components.

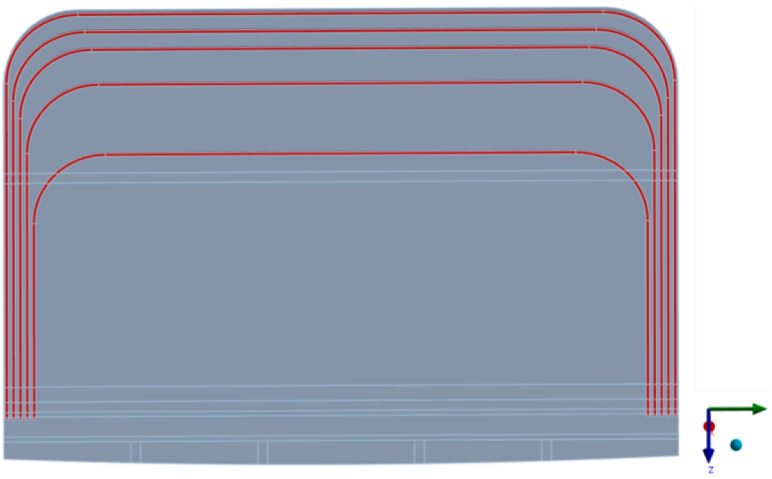

Fig. 9. TC cooling channels.

lower than 1%.

3.3. Nuclear analysis and obtained results

Adopting the MCNP model set-up, nuclear analysis has been run in order to calculate the radial trend of the nuclear volumetric heat power density and the power breakdown across the various materials. In particular, the power contribution relating to neutrons from the plasma and their progeny, as well as the photons they produce, is distinguished from the contribution relating to photons from the plasma chamber, that is coming from neutron interactions taking place elsewhere in the reactor. The former is named "n-p", and the latter "p". Obviously, these contributions always relate to two distinct analyses pertaining to two different sources: one neutron-related (transport analysis of neutrons and photons) and one photon-related (transport analysis of photons), as previously mentioned, developed with sampling based on a general input relating to DEMO. As an example, only results relevant to the Eurofer cassette option are shown. In this regard, the radial trends of the volumetric heat power density (q''') are depicted in Fig. 6 whereas the total deposited power breakdown is reported in Table 1, where the total deposited power in case of SiC cassettes is reported too for comparison. As one can observe, the total deposited power slightly increases (+ 3.5%) passing from Eurofer to SiC cassette option.

The so obtained radial profiles of volumetric heat power density can be used as input in thermal analysis, as already shown in the following.

4. Analysis of the thermo-mechanical behaviour of the Top Cap region

The thermo-mechanical performances of the Top Cap (TC) region of the WLCB BB COB segment, located in the COB Region 1 (Fig. 7), have been assessed under the expected steady-state normal operation loading scenario. With the aim of performing the analysis, a region encompassing the TC plate and 20 SB cooling channels have been extracted from the entire segment geometry. The study has been conducted adopting a numerical approach based on the Finite Element Method (FEM), using the commercial Ansys Workbench commercial code.

4.1. The geometric layout

The geometric details of the considered TC region are shown in Fig. 8. As already shown in neutronic analysis, the TC plate, FW, CSs, BSS and Vertical Stiffener (or Back Stiffener) are made in Eurofer. Instead, as to cassette and canister, Eurofer is the reference material but the possibility of using the SiC as alternative is considered in this work, since it allows to safely work at higher temperatures (up to ~1500 °C). Regarding the TC plate, it does not foresee any cooling channel in the baseline geometry. However, on the basis of the past experience [1,16] confirmed by preliminary analyses (not reported for the sake of brevity), the necessity to introduce cooling channels within the TC plate to properly limit the temperatures clearly emerged. Hence, 5 cooling channels have been added, as depicted in Fig. 9.

Differently from the geometric layout adopted for neutronic analysis (Fig. 2), the purge gas channels (formed by the join of cassettes with CSs, FW and back stiffener) have been considered in thermo-mechanical analysis (Fig. 8).

4.2. The developed 3D FEM model

In order to perform the thermo-mechanical analysis of the TC region of the WLCB BB COB segment, a dedicated 3D FEM model has been developed. First, a mesh of ~3.98 M nodes connected in ~4.06 M linear mixed (i.e. hexahedral, tetrahedral and wedge) elements has been generated on the geometric configuration shown before. A proper mesh constraint has been imposed where possible, in order to ensure the mesh continuity across bodies' interfaces. Instead, bonded contact models have been applied elsewhere.

Temperature-dependent material behaviour has been implemented for Eurofer [17], Tungsten [18], ACB [19,20], SiC [21,22] and Pb [23], assuming isotropic behaviour for all the materials.

From the thermal point of view, the following set of loads and boundary conditions has been implemented to perform the thermal analysis under the expected steady-state normal operation loading scenario:

- non-uniform Heat Flux (HF) radiated by the plasma;
- 3D nuclear volumetric power density;
- convective heat transfer conditions;
- imposed temperature onto the manifolds wetted surfaces;
- bonded contacts for cassettes;
- adiabatic purge gas channels and manifolds.

A non-uniform HF value has been applied onto the model plasma-facing surface, to simulate the plasma thermal radiation. In particular, a HF of 0.24 MW/m^2 has been applied onto the straight tungsten surface [24], decreasing to 0 onto the bends.

The non-uniform nuclear volumetric power density calculated for the WLCB COB segment equatorial region and scaled according to the Neutron Wall Loading poloidal distribution has been applied. In this regard, a scaling factor of 0.734 [25] has been assumed considering that the calculated power density values refer to Region 3 whereas the TC region is located in Region 1 (Fig. 7) of the WLCB BB COB segment. The

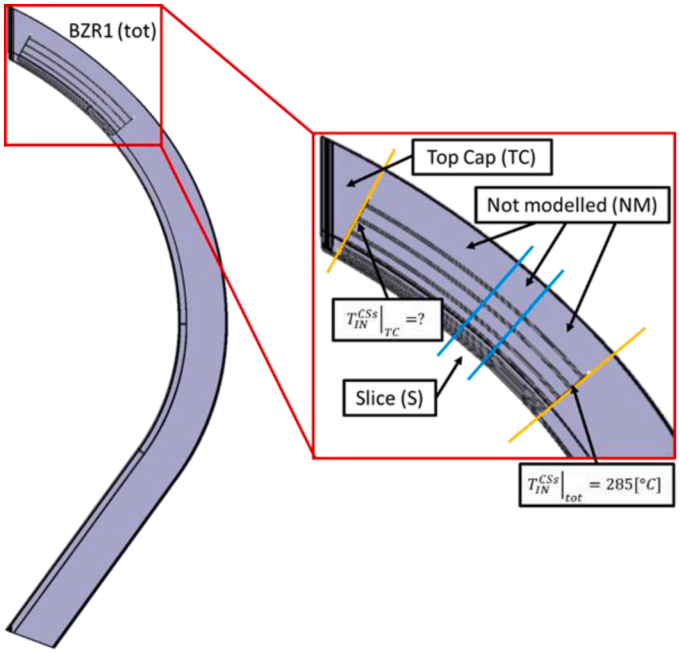

Fig. 10. Detail of the convective condition calculation.

specific power density spatial distributions have been assumed on the basis of the material selected for cassettes and canisters (Eurofer or SiC).

In order to simulate the forced convection phenomena occurring between cooling water and channels, the Ansys Workbench "thermal fluids" approach has been adopted. It allows representing the coolant by means of a one-dimensional body, discretised and coupled to the channel surfaces by means of a convective condition. Assigning to each thermal fluid body the fluid mass flow rate per unit area, the Heat Transfer Coefficient (HTC) and the bulk inlet temperature, the bulk temperature profile along the line is calculated and used for the convective boundary condition application. Therefore, the unique constant term of the imposed forced convective boundary condition is the HTC. A proper geometric parameter of the thermal fluid can be set to reproduce the coolant direction, so allowing the simulation of either co-current (such as in CSs) or counter-current (such as in SB) flow. Hence, in order to calculate the mass flow rates (MFRs) and the HTCs necessary to set the thermal fluids inside each channel, a purposely set-up analytical iterative procedure that considers coolant recirculation has been set-up and applied. It is based on the same approach described in [1].

The starting assumption is that the cooling water entering the Region 1 (called in the following BZR1) at the temperature of 285 °C cools down in series the CSs and, afterwards, the SB and TC channels after an intermediate mixing in a dedicated manifold. Hence, an intermediate mixing temperature will be achieved by the fluid at the CSs exit ($\overline{T}_{CSs}^{out}$), which can be assumed as the SB and TC channel inlet one. As the water enters the CSs from the bottom of the BZR1, the temperature of the water entering the portion of the CSs reproduced in the FEM model ($T_{IN}^{CSs}|_{TC}$) is unknown, since water is at 285 °C at the CSs entrance that is on the bottom of the BZR1 (Fig. 10), namely within the Not-Modelled (NM) BZR1 region. In the same way, also the mixing temperature at the CSs outlets, corresponding to the SB channels inlet one, has to be determined.

The BZR1 geometry houses 209 radial-toroidal-radial SB channels (n_{tot}^{SB}), 5 radial-toroidal-radial TC channels (n^{TopCap}) and 222 poloidal CSs channels (n^{CSs}). Observing that the modelled TC region includes only 20 channels (n_{TC}^{SB}), one can deduce that the NM BZR1 portion (i.e. the BZR1 region between the yellow lines in Fig. 10) houses 209 - 20 = 189, cooling channels (n_{NM}^{SB}). Then, the estimation of the heat power removed from the NM part of BZR1 is necessary to calculate the CSs water inlet temperature in the represented TC region, $T_{IN}^{CSs}|_{TC}$. To this scope, considering a Slice (S) of the NM portion (Fig. 10) housing 15 channels, one can see that the ratio between NM and S regions volumes (V_{NM} / V_S) amounts to 12.6 (i. e. 189 / 15 ≈ 12.6). Hence, the overall removed heat power in the different regions can be computed by analysis, so to have $\dot{Q}_S = \dot{Q}_S^{SB} + \dot{Q}_S^{CSs}$. Once obtained $\dot{Q}_S$, one can estimate the total BZR1 power $\dot{Q}_{tot}^0$as:

$$\dot{Q}_{tot}^0 = \dot{Q}_S \frac{V_{tot}}{V_S} = \dot{Q}_S \frac{V_{NM} + V_{TC}}{V_S} = \dot{Q}_S \frac{12.6 V_S + V_{TC}}{V_S} = \dot{Q}_S \left(12.6 + \frac{V_{TC}}{V_S}\right)$$

where V_{TC} is the volume of the modelled TC region. Then, the total power removed from the NM region, $\dot{Q}_{NM}$, can be together with the SB and CSs fractions:

$$\dot{Q}_{NM} = \dot{Q}_S \frac{V_{NM}}{V_S} = 12.6 \dot{Q}_S$$

$$\dot{Q}_{NM}^{SB} = \dot{Q}_S^{SB} \frac{V_{NM}}{V_S} = 12.6 \dot{Q}_S^{SB}$$

$$\dot{Q}_{NM}^{CSs} = \dot{Q}_S^{CSs} \frac{V_{NM}}{V_S} = 12.6 \dot{Q}_S^{CSs} = \dot{Q}_{NM} - \dot{Q}_{NM}^{SB}$$

At this point, the overall mass flow rate $\dot{m}_{tot}^0$ and the inlet temperature of the modelled CSs $T_{IN}^{CSs}|_{TC}$ can be evaluated as:

$$\dot{m}_{tot}^0 = \frac{\dot{Q}_{tot}^0}{\bar{c}_p (325 - 285)}$$

$$T_{IN}^{CSs}|_{TC} = 285 + \frac{\dot{Q}_{NM}^{CSs}}{\bar{c}_p \dot{m}_{tot}^0}$$

where 285 °C and 325 °C are the BZR1 water inlet and outlet temperatures and $\bar{c}_p$ is the average specific heat at constant pressure (15.5 MPa).

From $\dot{m}_{tot}^0$, the mass flow rate per SB and TC channel, $\dot{m}_{SB}^0$, and per CS channel, $\dot{m}_{CSs}^0$, can be obtained as:

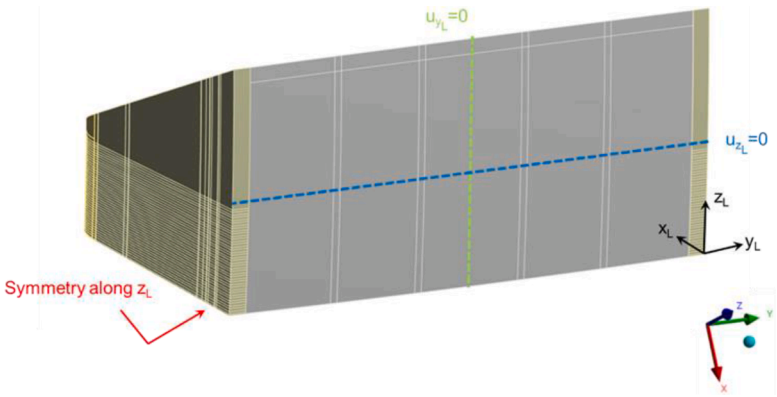

Fig. 11. Mechanical restraints.

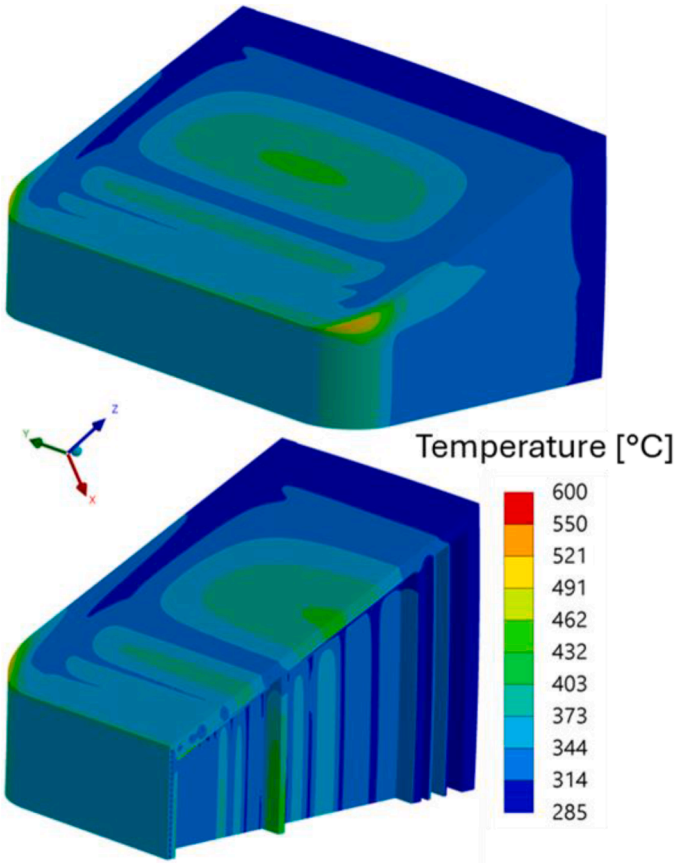

Fig. 12. Eurofer cassette option - thermal field within components with structural function.

$$\dot{m}^0_{SB} = \frac{\dot{m}^0_{tot}}{\left(n^{SB}_{tot} + n^{TopCap}\right)}$$

$$\dot{m}^0_{CSs} = \frac{\dot{m}^0_{tot}}{n^{CSs}}$$

Finally, one can find the HTC values adopting the Nusselt number, calculated by means of the Gnielinski correlation:

$$HTC^0_{SB} = \frac{Nu^0_{SB}\overline{k}}{D^{SB}_h}$$

$$HTC^0_{CSs} = \frac{Nu^0_{CSs}\overline{k}}{D^{CSs}_h}$$

where $\overline{k}$ is the water thermal conductivity at the average temperature and D_h is the hydraulic diameter of the considered channel.

At this point the thermal analysis of the TC region can be carried out and the power removed in SB and CSs can be calculated as:

$$\dot{Q}^1_{tot} = \dot{Q}^1_{SB} + \dot{Q}^1_{CSs} + \dot{Q}_{NM}$$

where $\dot{Q}^1_{SB}$ also includes the power removed by the 5 TC cooling channels (n^{TopCap}). At this point, $\dot{Q}^1_{tot}$ is compared to $\dot{Q}^0_{tot}$ and the procedure is iterated until $\dot{Q}^{n+1}_{tot} \approx \dot{Q}^n_{tot}$. Moreover, for each iteration, it has to be checked that the weighted average ($\overline{T}^{out}_{SB}|_{tot}$) between the mean temperature of the coolant exiting the modelled portion of SB and TC ($\overline{T}^{out}_{SB}|_{TC}$), obtained from the FEM thermal analysis, and the mean temperature of the coolant exiting the NM SB ($\overline{T}^{out}_{SB}|_{NM}$) converge to the target value of 325 °C. To this purpose, $\overline{T}^{out}_{SB}|_{NM}$ and $\overline{T}^{out}_{SB}|_{tot}$ are obtained as follows:

$$\overline{T}^{out}_{SB}|_{NM} = \overline{T}^{out}_{CSs} + \frac{\dot{Q}^{SB}_{NM}}{\overline{c}_p \dot{m}_{SB}\left(n^{SB}_{NM} + n^{TopCap}\right)}$$

$$\overline{T}^{out}_{SB}|_{tot} = \frac{\left(n^{SB}_{TC} + n^{TopCap}\right)\overline{T}^{out}_{SB}|_{TC} + n^{SB}_{NM}\overline{T}^{out}_{SB}|_{NM}}{n^{SB}_{tot} + n^{TopCap}}$$

Concerning the Eurofer cassette option, after a few iterations it has been found that, as to the SB and TC cooling channels, a MFR per channel of 0.090 kg/s and an HTC of 22343 W/(m2• °C) have been found, whereas regarding CSs channels a MFR of 0.087 kg/s and an HTC of 21565 W/(m2• °C) have been calculated. At the final iteration, a mixing temperature at the CSs exit $\overline{T}^{out}_{CSs}$ of 309. 4 °C is found.

Furthermore, as already mentioned, proper temperatures are imposed onto the manifolds wetted surfaces. Specifically:

- the inlet manifolds temperature set to 285 °C;
- the outlet manifolds temperature s set to 325 °C;
- the intermediate manifold temperature set to $\overline{T}^{out}_{CSs}$ that is calculated and imposed to manifolds nodes and used as TC and SB channels inlet temperature thanks to a purposely set-up Python script capable of managing the necessary Ansys APDL commands.

A perfect contact model is assumed between cassettes and the surrounding components, leaving to the following dedicated submodel analysis the investigation of the thermal contact resistance.

The purge gas manifold and channels have been assumed adiabatic.

From the structural standpoint, the normal operation loading scenario (classified as Level A in the RCC-MRx code [26]) has been properly characterised to perform the mechanical analysis defining:

- pressure loads;

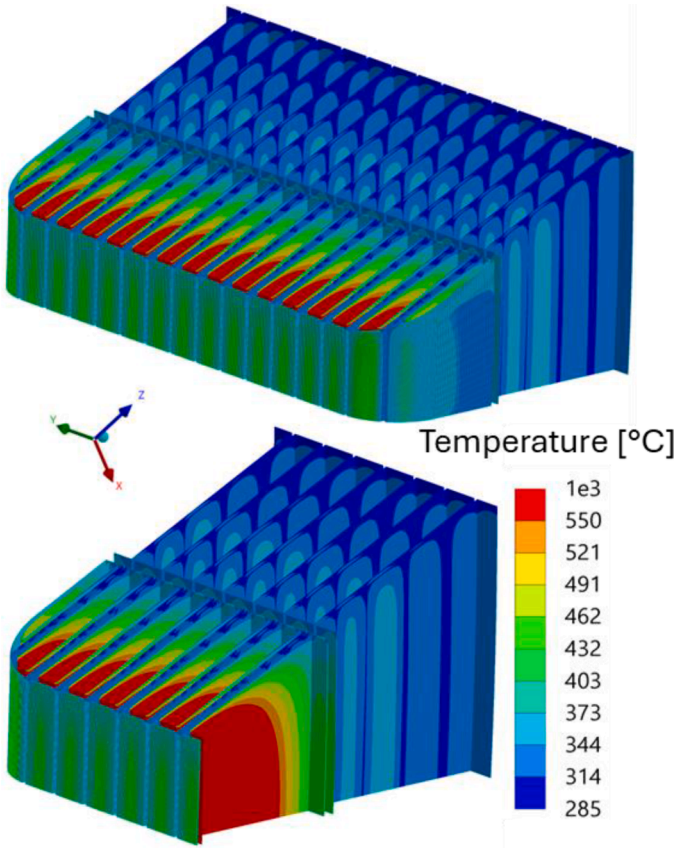

Fig. 13. Eurofer cassette option - thermal field within cassettes and canisters.

- non-uniform thermal deformation field;
- mechanical restraints;
- bonded contacts for cassettes.

A pressure load of 15.5 MPa has been applied within the SB, CSs and TC channels and the manifolds. Instead, to consider the effect of the purge gas, a pressure of 0.2 MPa has been imposed onto the purge gas wetted surfaces. Finally, with regard to the surfaces in contact with the lead, a pressure of 0.045 MPa has been imposed.

The 3D spatial distribution of the temperature already obtained in the first phase of the study, has been applied to the assessed region, differing between SiC and Eurofer cassette options.

As to the mechanical boundary conditions, symmetry has been applied to the lower surface of the considered region, to consider the effect of the entire segment. Moreover, displacements along local Y and Z direction have been prevented to selected nodes onto the back plate to simulate the action of a supporting system, as shown in Fig. 11. Lastly, as already done in thermal analysis, perfect contact has been assumed between cassettes and surrounding components, leaving to the following submodel analysis the evaluation of the effect of a frictional contact between cassettes and surrounding components.

4.3. Thermo-mechanical analysis and obtained results

Steady-state thermal analyses considering both Eurofer and SiC cassette options have been performed. Since qualitatively similar results are obtained, for the sake of brevity only thermal fields obtained in case of Eurofer cassettes are reported. In particular, looking at those components having structural function (namely the SB, the BSS, the stiffeners and the TC), the predicted temperature spatial distribution (Fig. 12) shows values quite lower than 550 °C, that is the suggested limit temperature for Eurofer.

In particular, a maximum temperature of 519 °C is obtained suggesting that the TC regions is compliant with the thermal requirement. Instead, the most interesting result regards the cassettes and canister domain, whose thermal field is reported in Fig. 13.

In both options, the maximum temperature value is similar (1000 °C within Eurofer and 971 °C within SiC). In particular, the highest temperatures are reached within the canisters which, unlike the cassettes, are not cooled. Since SiC can safely work up to ~1500 °C, only in the Eurofer cassette option the thermal requirement is not fulfilled, even

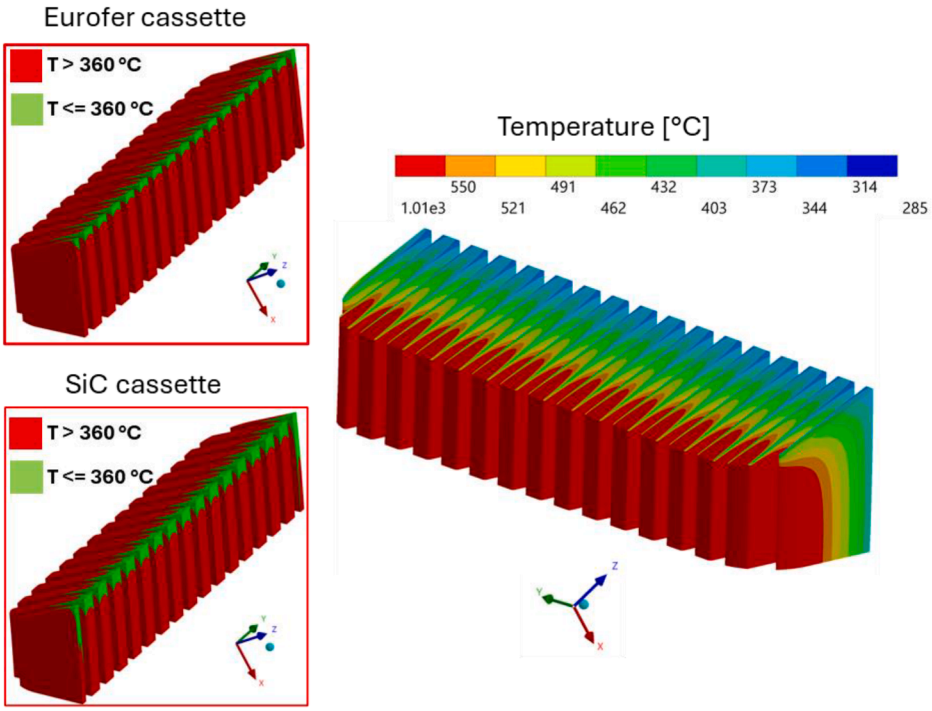

Fig. 14. Eurofer cassette option - thermal field within lead.

Table 2
Considered RCC-MRx criteria [26].

Damage mode	Criterion
Imm. Excess. Deform.	P_m / S_m
Imm. Plastic Inst.	(P_m + P_b) / 1.5S_m
Imm.ediate Plastic Flow Loc.	(P_m + Q_m) / S_{em}
Imm. Fract. due to Exhaust. of Duct.	(P_m + P_b + Q + F) / S_{et}

though canisters do not have any structural role and therefore the requirement on the maximum temperature may not be so strict. Possible solutions to this issue might be an intermediate design choice, foreseeing Eurofer for cassettes and SiC for canisters, or the swap of ACB and Pb with respect to the canister that could imply a mitigation of the temperatures in the Eurofer cassette option.

Another important aspect emerging from thermal analysis regards the molten lead thermal field. Instead, as shown in Fig. 14, the top region experiences temperature quite close to the melting point (327.5 °C), deserving a more detailed analysis. As one can observe, the critical region extends in case of SiC cassette. This result means that a dedicated analysis is necessary to deeply assess the lead thermofluid-dynamic behaviour in the TC region. In addition, the high temperature achieved within Pb domain are due to the fact that it can loss heat only by diffusion through the canister, that is a very poor heat removal way. Therefore, the swap of ACB and lead with respect to the canister could help in solving this issue too.

From the structural standpoint, static analysis allowed evaluating the component's mechanical performances. In this regard, the fulfilment of the RCC-MRx Level A structural design criteria reported in (Table 2) has been checked. To this scope, a stress linearization procedure has been performed along 5 paths throughout the Top Cap plate thickness (Fig. 15).

The results, shown in Fig. 15 as ratios between the equivalent stress and its limit, allow concluding that the TC plate is able of safely withstanding the nominal loading conditions with a remarkable margin independently from the material selected for the cassette.

The evaluation of the FW and CSs structural performances in view of the considered code has been performed in the dedicated submodel analysis, where a more realistic behaviour is predicted thanks to the consideration of the non-ideal nature of the contact between cassettes and structural components.

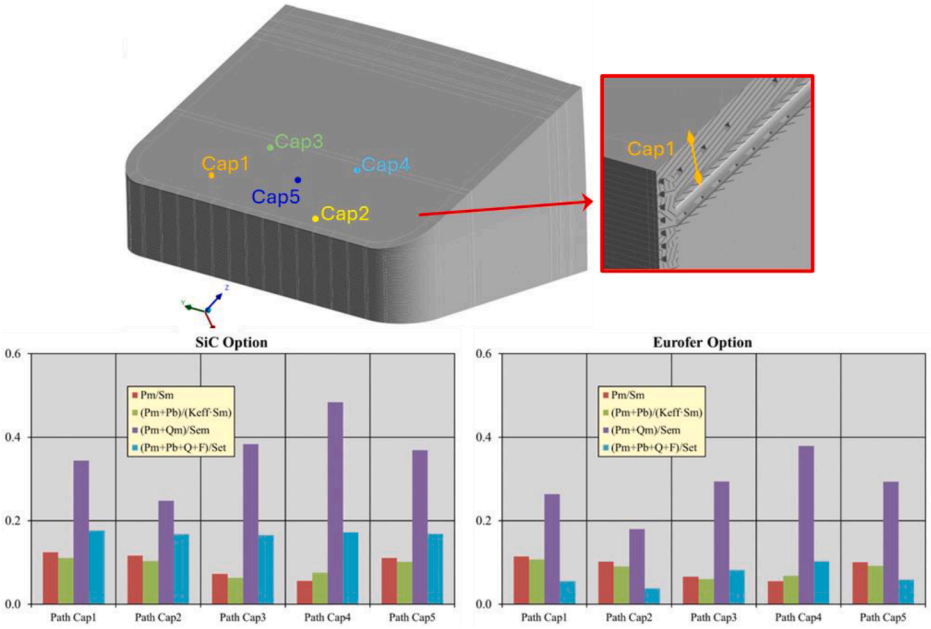

Fig. 15. Selected paths within the TC and RCC-MRx Level A criteria verification.

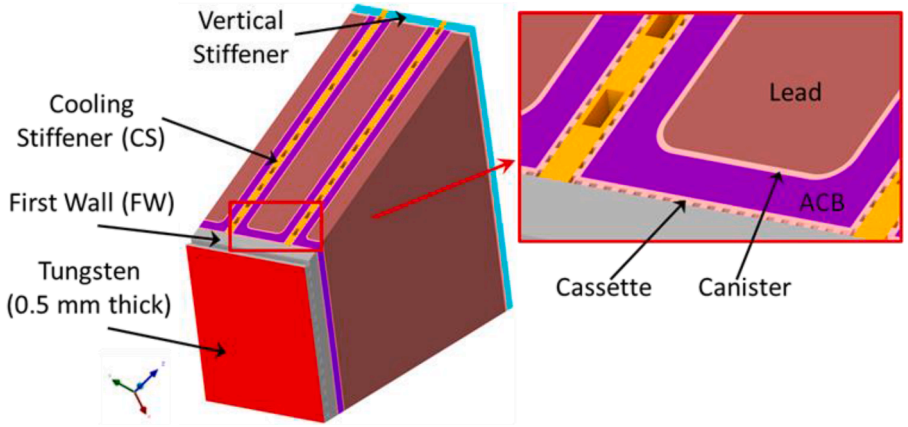

Fig. 16. Submodel geometric details.

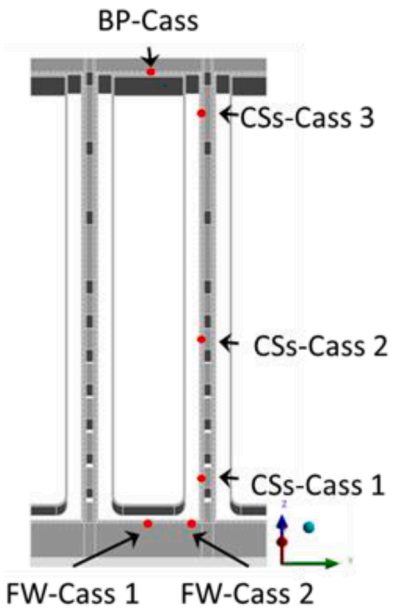

Fig. 17. Temperature monitoring points.

5. Local thermo-mechanical analysis

In order to evaluate more realistically the thermal and structural performances of the TC region of the WLCB BB COB segment, specifically considering the non-ideal contact between the cassettes and the surrounding components, a campaign of submodel thermo-mechanical analysis has been performed. To this purpose, a specific submodel has been extracted from the geometric configuration shown in Fig. 8 and the temperature and displacement previously calculated (from the analysis described in Section 4) have been mapped at the cutting surfaces as submodel's boundary conditions.

5.1. The geometric model

In order to perform the submodel analysis, the geometric layout depicted in Fig. 16 has been considered. Both Eurofer and SiC cassette options have been investigated.

5.2. The 3D FEM model

With the aim of performing the detailed thermal and structural analyses of the submodel region, the corresponding 3D FEM models have been set-up. A totally connected the mesh, made of ~2.70 M nodes connected in ~590k quadratic hexahedral and wedge elements, has been generated.

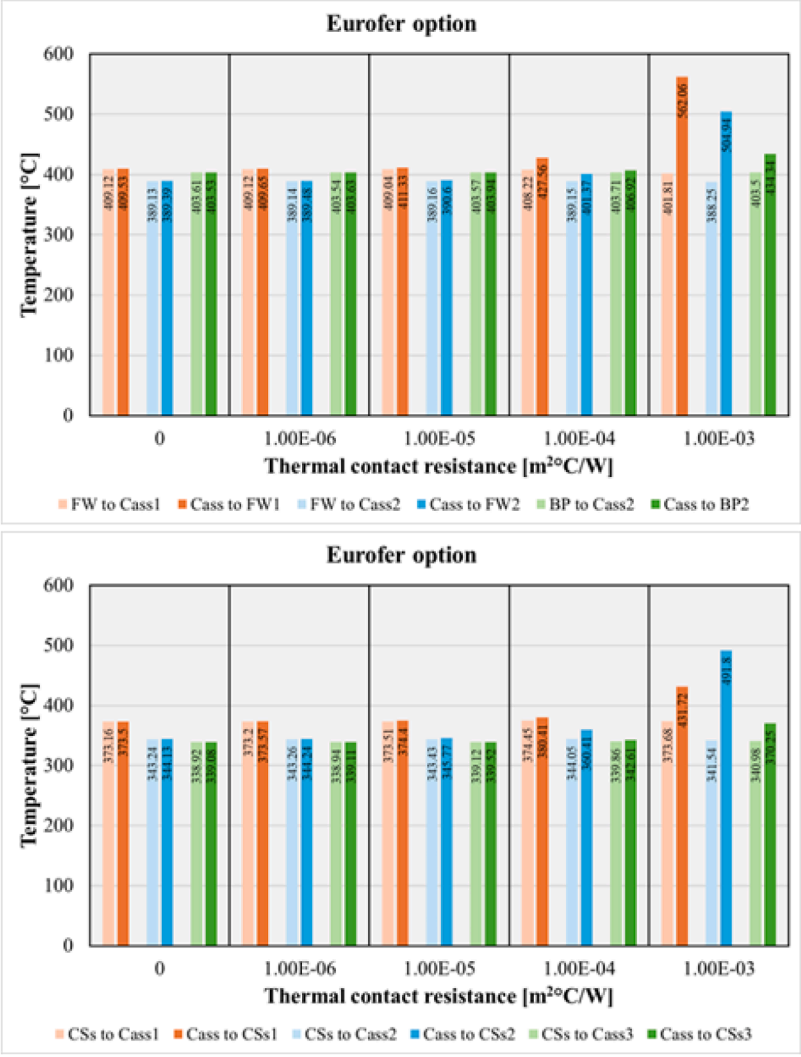

Fig. 18. Effect of the assumed thermal contact resistance on the temperature of monitoring points.

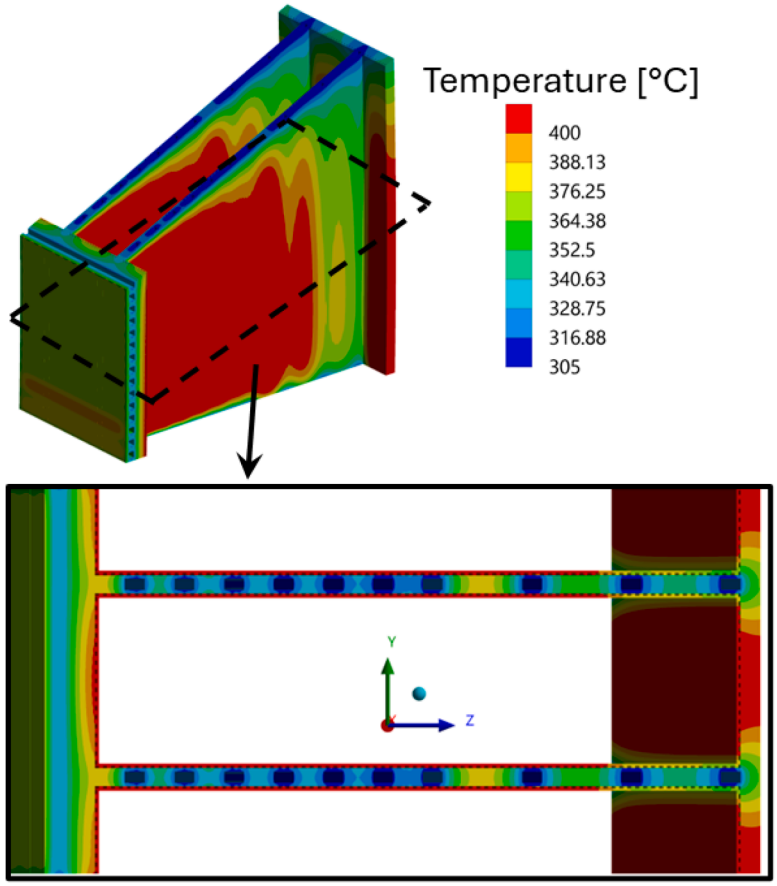

Fig. 19. Eurofer cassette option – R = 1.0 E-03 m^2• °C/W – Thermal field.

Concerning the loads and boundary conditions aimed at representing the normal operation loading scenario, from the thermal point of view the same non-uniform HF, nuclear power density, convective heat transfer condition and imposed temperatures onto the manifolds as the model used for the assessment of the whole TC region have been imposed. In addition, the temperature values previously calculated have been mapped onto the submodel cutting surfaces. Moreover, in order to increase the level of detail, different values of the contact thermal resistance (R) between cassettes and surrounding components have been assumed. In particular, 5 values equally spaced in the range 0 - 1.0 E-03 m^2• °C/W have been [27]. The same range has been considered for both SiC and Eurofer cassette options. The necessity to consider a thermal contact resistance in the contact between cassettes and structural components (FW, CSs and vertical stiffener) comes from the fact that the cassettes are not welded, but they can slide within the BB segment up to their final position. Hence, a certain surface roughness is expected, and the resulting voids can be filled by the purge gas flowing through the channels created by the interface between cassettes and structural components (Fig. 16). In this regard, it is important to note that assuming a purge gas (namely helium at 0.2 MPa and 450 °C) thermal conductivity of ~0.29 W/(m• °C), a contact thermal resistance of 1.0 E-03 m^2• °C/W corresponds to an average gap between the contact surfaces of ~290 μm. Typical roughness values for such kind of component usually do not exceed 200 μm. Therefore, the assumption of a contact thermal resistance value equal 1.0 E-03 m^2• °C/W allows to be largely conservative in this regard.

From the mechanical point of view, the same pressure loads as the global TC region model have been considered. In addition, the purge gas pressure has been imposed also within the channels created by the cassettes and the structural components. Moreover, the thermal fields calculated in the thermal submodel analyses have been imported and, as to boundary conditions, the displacement field calculated in the TC region analysis has been mapped onto the submodel cutting surfaces. Finally, a frictional contact model has been applied between cassettes and surrounding components. A friction factor of 0.74 for Eurofer cassette [28] and of 0.35 for SiC cassette [22] has been used.

5.3. Submodel analysis and obtained results

Steady-state thermal analyses of the TC region submodel under the nominal loading conditions for both Eurofer and SiC cassette have been performed. Since qualitatively similar results are obtained, for the sake of brevity only those concerning Eurofer cassettes are reported. Six monitoring points have been selected (Fig. 17) to assess the impact of the considered R values onto the thermal field. Results (Fig. 18) allow concluding that values of R up to 1.0 E-05 m^2• °C/W do not produce any significant temperature drop across the contact whereas a moderate influence is detected for R = 1.0 E-04 m^2• °C/W and a strong impact is obtained if thermal contact resistance increases of another order of magnitude (up to 1.0 E-03). Hence, for the sake of brevity, only the thermal field obtained for the Eurofer cassette option for the highest R value (1.0 E-03 m^2• °C/W) is shown in the following (Fig. 19). As one can observe, also in the case of the highest (quite conservative) R value, the highest temperatures are predicted within cassettes (where a maximum of ~ 600 °C is achieved) whereas the CSs, the FW and the vertical stiffener are colder than 500 °C. Qualitatively similar results are obtained for the SiC cassette option too, confirming that also introducing a non-ideal behaviour for the cassettes contact the thermal performances of the structural components are compliant with the requirements. In case of SiC cassettes, the predicted temperature values allow confirming that no issues arise for this component too.

A static analysis has been performed under the above-mentioned

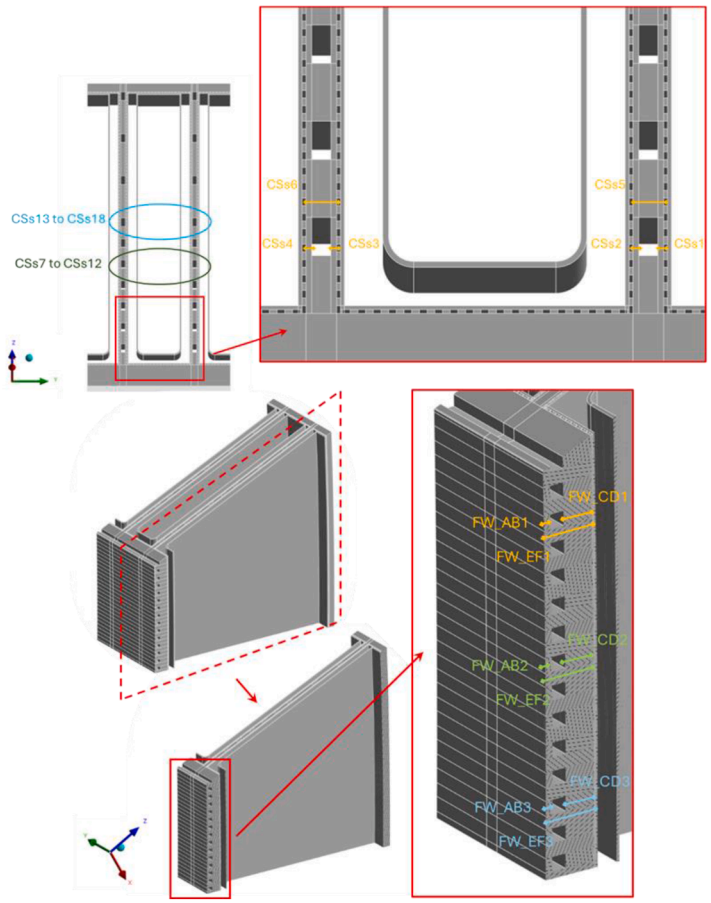

Fig. 20. Paths within FW and CSs.

nominal loading conditions, with the aim of evaluating the structural response of the FW and CSs under more realistic conditions. In this regard, the fulfilment of the RCC-MRx Level A structural design criteria reported in Table 2 has been checked using the set of paths located within the FW and the CSs shown in Fig. 20. Globally, it has been observed that the structural performances slightly worsen when the thermal contact resistance increases. This is because an increase of R produces an average increase of the cassette temperature, that in turn expands more and stresses more the FW and CSs.

For the sake of brevity, only results concerning the case with – R = 1.0 E-03 m2● °C/W are shown as it represents the most conservative one. In particular, as to FW, the outcomes of the RCC-MRx criteria verification for both the assessed options are shown in Fig. 21. As one can observe, the SiC cassette ensures a global fulfilment of the selected criteria within FW, even though with a narrow margin in some cases. On the other hand, criteria are not totally met in the case of Eurofer cassette with values slightly over the limit. Hence, in both cases, one can conclude that the global fulfilment of the Level A criteria is borderline. Instead, as to the CSs, the situation is overturned (Fig. 22). These preliminary results are encouraging, even though more refined analyses are necessary to consider the impact of friction factors, mesh quality and adopted constitutive models for the structural material onto the WLCB BB structural component.

6. Conclusion

The campaign of analysis herein presented allowed confirming the good aptitude of the DEMO WLCB BB concept to fulfil project requirements. However, a follow up is necessary to finalise its layout, with a particular attention to the breeding zone. Moreover, cost and manufacturing issues might prevent the adoption of SiC for both cassettes and canisters. Regarding the Top Cap, the current architecture with 5 cooling channels can be assumed as the reference. The design solutions considered in this work need to be extrapolated to conceive an entire BB segment that should be assessed in the close future. In addition, some possible design modifications (swap of the functional materials within the cassette, double material for cassette and canister) deserve to be investigated by means of dedicated campaign of analysis. From an overall point of view, the obtained results represent a very promising starting point.

CRediT authorship contribution statement

G. Bongiovì: Conceptualization, Data curation, Formal analysis, Investigation, Methodology, Software, Supervision, Validation, Visualization, Writing – original draft, Writing – review & editing. **P. Chiovaro:** Conceptualization, Data curation, Formal analysis, Investigation, Methodology, Software, Supervision, Validation, Visualization, Writing – original draft, Writing – review & editing. **I. Catanzaro:** Conceptualization, Data curation, Formal analysis, Investigation, Methodology, Software, Supervision, Validation, Visualization, Writing – original draft, Writing – review & editing. **S. Maggio:** Conceptualization, Data curation, Formal analysis, Investigation, Methodology, Software, Supervision, Validation, Visualization, Writing – original draft, Writing – review & editing. **F.A. Hernandez:** Conceptualization, Data curation, Formal analysis, Investigation, Methodology, Software, Supervision, Validation, Visualization, Writing – original draft, Writing – review & editing. **S. D'Amico:** Conceptualization, Data curation, Formal analysis, Investigation, Methodology, Software, Supervision, Validation, Visualization, Writing – original draft, Writing – review & editing. **E. Vallone:**

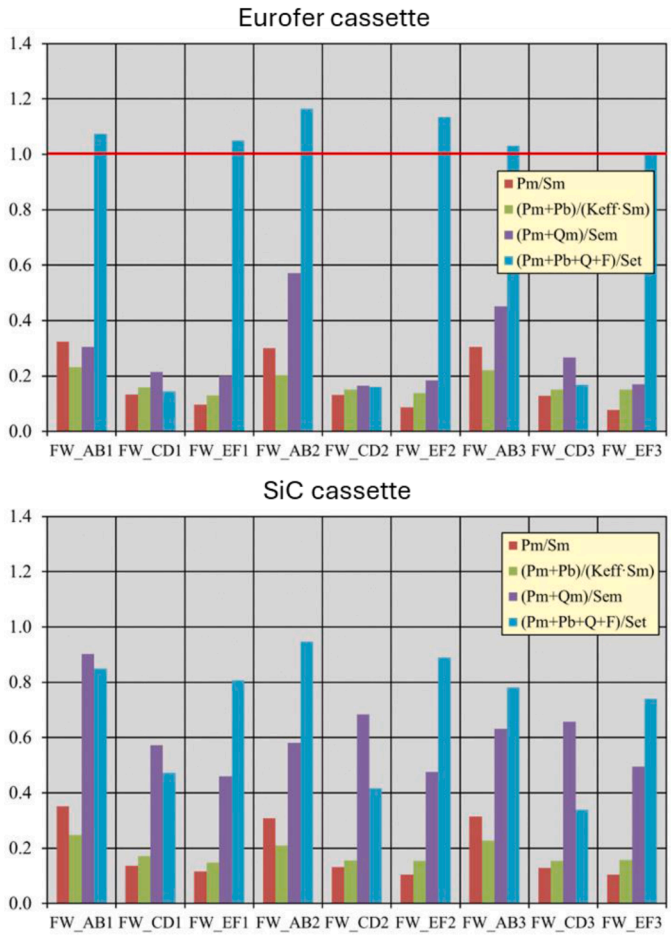

Fig. 21. RCC-MRx Level A criteria verification - FW.

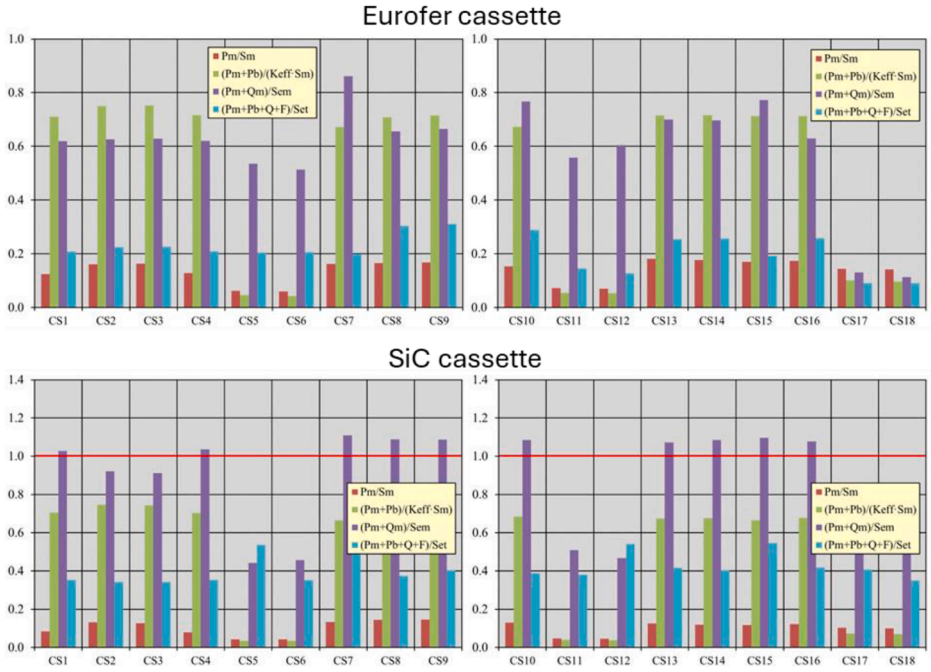

Fig. 22. RCC-MRx Level A criteria verification - CSs.

Conceptualization, Data curation, Formal analysis, Investigation, Methodology, Resources, Software, Supervision, Validation, Visualization, Writing – original draft, Writing – review & editing. **P.A. Di Maio:** Conceptualization, Data curation, Formal analysis,

Investigation, Methodology, Software, Supervision, Validation, Visualization, Writing – original draft, Writing – review & editing.

Declaration of competing interest

The authors declare that they have no known competing financial interests or personal relationships that could have appeared to influence the work reported in this paper.

Acknowledgement

This work has been carried out within the framework of the EUROfusion Consortium, funded by the European Union via the Euratom Research and Training Programme (Grant Agreement No 101052200—EUROfusion). Views and opinions expressed are however those of the author(s) only and do not necessarily reflect those of the European Union or the European Commission. Neither the European Union nor the European Commission can be held responsible for them.

Data availability

Data will be made available on request.

References

[1] F. Hernandez, et al., Advancements in designing the DEMO driver blanket system at the EU DEMO pre-conceptual design phase: overview, challenges and opportunities, J. Nucl. Eng 4 (2023) 565–601, https://doi.org/10.3390/jne4030037.
[2] G. Federici, et al., The EU DEMO staged design approach in the pre-concept design phase, Fusion Eng. Des. 173 (2021) 112959, https://doi.org/10.1016/j.fusengdes.2021.112959.
[3] G. Zhou, et al., A water cooled lead ceramic breeder blanket for European DEMO, Fusion Eng. Des. 168 (2021) 112397, https://doi.org/10.1016/j.fusengdes.2021.112397.
[4] Y. Lu, et al., Exploratory tritium breeding performance study on a water cooled lead ceramic breeder blanket for EU DEMO using Serpent-2, Nucl. Mater. Energy 28 (2021) 101050, https://doi.org/10.1016/j.nme.2021.101050.
[5] P. Pereslavtsev, et al., Neutronic activity for development of the promising alternative water-cooled DEMO concepts, Appl. Sci. 13 (2023) 7383, https://doi.org/10.3390/app13137383.
[6] S. Giambrone, et al., Preliminary thermo-mechanical assessment of the Top Cap region of the water-cooled lead-ceramic breeder breeding blanket alternative concept, Fusion Eng. Des. 200 (2024) 114201, https://doi.org/10.1016/j.fusengdes.2024.114201.
[7] I. Palermo, et al., Water-cooled lead and ceramic breeder (WLCB) breeding blanket (BB) for the EU DEMO: neutronic campaigns for T breeding optimization, Nucl. Mater. Energy 45 (2025) 102022, https://doi.org/10.1016/j.nme.2025.102022.
[8] F. Hernandez, EUROfusion PMU, personal communication, 2025.
[9] X-5 Monte Carlo Team, MCNP – A General Monte Carlo N-Particle Transport Code, 2003, LANL, Los Alamos, New Mexico, USA, April 2003. Version 5.
[10] NEA, JEFF3.3, Nucl. Data Libr. (2017). https://oecd-nea.org/dbdata/jeff/jeff33/#neutron.
[11] Y. Wu, et al., CAD-based Monte Carlo program for integrated simulation of nuclear system SuperMC, Ann. Nucl. Energy 82 (2015) 161–168, https://doi.org/10.1016/j.anucene.2014.08.058.
[12] G.A. Spagnuolo, et al., A multi-physics integrated approach to breeding blanket modelling and design, Fusion Eng. Des. 143 (2019) 35–40, https://doi.org/10.1016/j.fusengdes.2019.03.131.
[13] P. Chiovaro, et al., Investigation of the DEMO WCLL breeding blanket cooling water activation, Fusion Eng. Des. 157 (2020) 111697, https://doi.org/10.1016/j.fusengdes.2020.111697.
[14] R. Favetti, et al., Validation of multi-physics integrated procedure for the HCPB breeding blanket, Int. J. Comput. Methods 17 (2020) 1950009, https://doi.org/10.1142/S0219876219500099.
[15] U. Fischer, Y. Qiu, Material Compositions for PPPT Neutronics and Activation Analyses, EUROfusion IDM Ref.: 2MM3A6, 2020 v1.1.
[16] P.A. Di Maio, et al., Thermo-mechanical analysis and design update of the Top Cap region of the DEMO water-cooled Lithium Lead Central outboard blanket segment, Appl. Sci. 12 (3) (2022) 1564, https://doi.org/10.3390/app12031564.
[17] E. Gaganidze, Material Properties Handbook – EUROFER97, IDM Ref.: EFDA_D_2NZHBS, 2020.
[18] E. Gaganidze, F. Schoofs, Material Properties Handbook – Tungsten, IDM Ref.: EFDA_D_2P3SPL, 2020.
[19] G. Zhou, et al., HCPB Design and Analysis – Interim Report 2021, IDM Ref.: EFDA_D_2Q4YMC, 2022 (v1.0).
[20] J.M. Leys, et al., Material Property Handbook On Advanced Ceramic Breeder (MAR/MDBR Update For ACB – Final report), IDM Ref.: EFDA_D_2NVAS9, 2019 (v1.0).
[21] R. Petráš, Mechanical and Electrical Characterization of Ceramics in an Inert Atmosphere and Pb-16Li, IDM Ref.: EFDA_D_2RSEDT, 2025. Technical report.
[22] Lance L. Snead, et al., Handbook of SiC properties for fuel performance modeling, J. nucl. mater. 371 (2007) 329–377, https://doi.org/10.1016/j.jnucmat.2007.05.016.
[23] Handbook On Lead-bismuth Eutectic Alloy and Lead Properties, Materials Compatibility, Thermal-hydraulics and Technologies, IEA, 2015.
[24] F. Maviglia, DEMO PFC Surface Heat Load Specifications, IDM Ref.: EFDA_D_2P985Q, 2020 v1.8.
[25] P. Arena, et al., WCLL BB Design Activities –2022 ENEA Contribution, IDM Ref.: EFDA_D_2QSA7X, 2023. Final Report on Deliverable.
[26] RCC-MRx, Design and Construction Rules For Mechanical Components of Nuclear Installations, AFCEN, Courbevoie, France, 2013.
[27] P.A. Di Maio, et al., Thermofluid-dynamic and thermal–structural assessment of the EU-DEMO WCLL "double bundle" Breeding Blanket concept left outboard segment, Fusion Eng. Des. 202 (2024) 114335, https://doi.org/10.1016/j.fusengdes.2024.114335.
[28] J.A. Noguerón, et al., Numerical investigation of the structural performances of the EU-DEMO Water-cooled Lead lithium breeding blanket equipped with helicoidal double-walled tubes, Fusion Eng. Des. 208 (2024) 114703, https://doi.org/10.1016/j.fusengdes.2024.114703.